



HAL
open science

High performance direct borohydride fuel cell using bipolar interfaces and noble metal-free Ni-based anodes

Guillaume Braesch, Zhongyang Wang, Shrihari Sankarasubramanian, Alexandr Oshchepkov, Antoine Bonnefont, Elena R Savinova, Vijay Ramani, Marian Chatenet

► To cite this version:

Guillaume Braesch, Zhongyang Wang, Shrihari Sankarasubramanian, Alexandr Oshchepkov, Antoine Bonnefont, et al.. High performance direct borohydride fuel cell using bipolar interfaces and noble metal-free Ni-based anodes. *Journal of Materials Chemistry A*, 2020, 8, pp.20543 - 20552. 10.1039/D0TA06405J . hal-02953350

HAL Id: hal-02953350

<https://hal.univ-grenoble-alpes.fr/hal-02953350v1>

Submitted on 30 Sep 2020

HAL is a multi-disciplinary open access archive for the deposit and dissemination of scientific research documents, whether they are published or not. The documents may come from teaching and research institutions in France or abroad, or from public or private research centers.

L'archive ouverte pluridisciplinaire **HAL**, est destinée au dépôt et à la diffusion de documents scientifiques de niveau recherche, publiés ou non, émanant des établissements d'enseignement et de recherche français ou étrangers, des laboratoires publics ou privés.

ARTICLE

High performance direct borohydride fuel cell using bipolar interfaces and noble metal-free Ni-based anodes

Guillaume Braesch^{1,2}*, Zhongyang Wang³, Shrihari Sankarasubramanian⁴, Alexandr G. Oshchepkov^{2,5}, Antoine Bonnefont⁶, Elena R. Savinova², Vijay Ramani⁴, Marian Chatenet^{1*}

Received 00th January 20xx,
Accepted 00th January 20xx

DOI: 10.1039/x0xx00000x

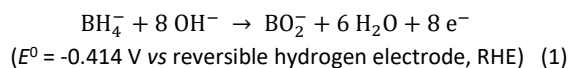
Due to its unmatched theoretical voltage of 2.18 V, direct alkaline fuel cell using sodium borohydride solution at the anode and hydrogen peroxide at the cathode, represents a promising power source for high energy density applications. However, its development faces several challenges. Here we demonstrate a $\text{BH}_4^-/\text{H}_2\text{O}_2$ direct borohydride fuel cell (DBFC) with a platinum group metal (PGM)-free anode, which delivers unprecedented combination of 2.0 V open-circuit voltage and peak power density of 446 mW cm^{-2} . This exceptionally high cell voltage is enabled by combining a pH-gradient-enabled microscale bipolar interface (PMBI), a Ni anode obtained by electrodeposition of Ni nanoparticles on an electrochemically-etched Ni felt (eNFT), and a specially-designed simple but efficient coating procedure to deposit anion-exchange ionomer on the anode surface. The PMBI efficiently separates the drastically-disparate pH of the anolyte and the catholyte, the Ni_{ED} /eNFT anode provides high surface area for efficient electrocatalysis and open porosity for fast mass-transport, while the coating procedure allows preserving Ni in metallic state, the latter being prerequisite for high anode performance. This work details how such fully nickel-based anodes are obtained and demonstrates why their BOR activity and stability outperforms that of PGM-based anodes.

KEYWORDS. Borohydride Oxidation Reaction (BOR), Direct Borohydride Fuel Cell (DBFC), Alkaline Fuel Cell (AFC), PGM-free anode, Bipolar interface, Hydrogen peroxide.

Introduction

Sodium borohydride (NaBH_4) is investigated since twenty years as a fuel for alkaline fuel cells.^{1–8} Advantages of NaBH_4 as a fuel are its ability to provide 8 electrons per BH_4^- anion (if fully oxidized in the Borohydride Oxidation Reaction, BOR, Equation 1), and its low standard potential translating in the high theoretical cell voltage of 1.64 V when O_2 is used as an oxidant. The latter exceeds the theoretical voltage of a Proton Exchange Membrane Fuel Cell (PEMFC, the present state-of-the-art system) by 0.41 V, making

Direct Borohydride Fuel Cell (DBFC), a promising technology for high-energy applications:



Besides, NaBH_4 is easily stored and transported in solid form and can be fed as liquid alkaline anolyte, ensuring safety of usage without compromising the high energy-density of the fuel. In the meantime, feeding H_2 in PEMFCs involves multiple technical difficulties of production, purification, compression, transport, not to speak of the safety and cost of these processes. Furthermore, hydrogen peroxide (H_2O_2) can be used as an oxidant, leading to a fully-liquid-fed system, the so-called $\text{BH}_4^-/\text{H}_2\text{O}_2$ DBFC^{3,9–12} with its unmatched theoretical

¹ University Grenoble Alpes, University Savoie Mont Blanc, CNRS, Grenoble INP (Institute of Engineering and management, University Grenoble Alpes), LEPMI, 38000 Grenoble, France

² Institut de Chimie et Procédés pour l'Energie, l'Environnement et la Santé, UMR 7515 CNRS-University of Strasbourg, 67087 Strasbourg Cedex, France

³ Pritzker School of Molecular Engineering, University of Chicago, Chicago, IL 60637, USA

⁴ Center for Solar Energy and Energy Storage and Department of Energy, Environmental and Chemical Engineering, McKelvey School of Engineering, Washington University in St. Louis, St. Louis, MO, USA.

⁵ Borekov Institute of Catalysis, 630090 Novosibirsk, Russia

⁶ Institut de Chimie de Strasbourg, UMR 7177 CNRS-University of Strasbourg, 67070 Strasbourg, France† Footnotes relating to the title and/or authors should appear here.

* Correspondence and material requests should be addressed to Marian Chatenet (Marian.Chatenet@grenoble-inp.fr) and Guillaume Braesch (Guillaume.Braesch@lepmi.grenoble-inp.fr).

Electronic Supplementary Information (ESI) available: [details of any supplementary information available should be included here]. See DOI: 10.1039/x0xx00000x

voltage of 2.18 V.¹ These attractive features make the $\text{BH}_4^-/\text{H}_2\text{O}_2$ DBFC an ideal technology for portable and mobile applications, e.g. in confined situations (such as submarines) where the use of H_2 may be dangerous. However, despite exceptional promises of the $\text{BH}_4^-/\text{H}_2\text{O}_2$ DBFC, practical implementation of such systems has not been achieved yet, essentially because of two hurdles.

The first obstacle is related to the difficulty in maintaining grossly different pH at the cathode fed with acidic H_2O_2 (the latter only being stable at low pH) and the anode fed with alkaline NaBH_4 solution (BH_4^- anions only being stable at high pH^{13,14}). Continuous operation requires maintaining the pH of both the catholyte and anolyte close to their original values (ca. 0 and 14, respectively) to avoid compromising the DBFC performance. Neither cation-exchange membranes (CEM) nor anion-exchange membranes (AEM)^{15–19}, which are used in DBFCs, are capable to maintain such pH gradient between the two electrodes. Bipolar interfaces (BI) developed for various application targets^{20–23} seem to offer significant advantages for $\text{BH}_4^-/\text{H}_2\text{O}_2$ DBFCs.^{24–26} Some of us¹⁹ have recently been able to significantly increase the open circuit voltage (OCV) of the $\text{BH}_4^-/\text{H}_2\text{O}_2$ DBFC by creating a “pH-gradient microscale bipolar interface (PMBI)”²⁷ that allows to maintain the pH gradient between the two electrodes. This enabled reaching a large peak power density of 300 $\text{mW}\cdot\text{cm}^{-2}$ and high OCV of 1.8 V for a 5 cm^2 unit $\text{BH}_4^-/\text{H}_2\text{O}_2$ DBFC with a Pd anode. Note however that the achieved OCV was still largely inferior to the theoretical OCV of 2.18 V.

The second obstacle, which hinders achieving high OCV and hence high energy density, is related to the utilization of PGMs at the DBFC anode. Known for their high hydrogen evolution reaction (HER) activity, PGMs prevent anode potential to extend below 0 V vs RHE, where the HER competes with the BOR. As a result, from 20 to 30% (depending on the oxidant used) of the theoretical cell voltage is lost with PGM-based electrocatalysts, not to mention their poor availability and high price²⁸.

In this work we demonstrate unprecedented $\text{BH}_4^-/\text{H}_2\text{O}_2$ DBFC performance, namely OCV reaching 2.0 V and peak power density of ca. 450 $\text{mW}\cdot\text{cm}^{-2}$, by combining a Ni-based anode and a pH-gradient-enabled microscale bipolar interface. In order to do so, we develop a

highly-efficient stand-alone 3D-shaped and surface-controlled Ni-based anode by electrodepositing Ni on an etched Ni felt with open porosity. We demonstrate that such an anode greatly outperforms either Ni catalysts prepared by conventional wet chemistry methods, or noble metal-based state-of-the-art catalyst materials. Electrodeposition, contrary to wet chemical methods, allows avoiding the passivation step, the latter resulting in oxidation of the Ni surface and ultimately to the BOR activity loss. We further design a PMBI preparation procedure, which allows preserving the surface of the Ni anode in an essentially metallic state, a determining factor allowing high BOR activity and high OCV.²⁹ Indeed, Ni had long been tested for the BOR, the reported activity oscillating between low^{30–32} and high values^{33–35}, until some of us demonstrated that these drastic differences of the observed activity originated from a poorly-controlled state-of-surface of the catalyst, as detailed in^{29,36–38}. When nickel is covered by an oxide layer, both its HER and BOR activity are vanishingly-low. However, if the state of the surface is controlled and maintained metallic, the BOR activity increases, while the HER activity remains small, resulting in a record-low onset potential (-0.25 V vs RHE, for $[\text{NaBH}_4] = 5 \text{ mM}$). In the meantime, the BOR kinetics is very fast on metallic nickel: the diffusion-limited current is reached below 0 V vs RHE²⁹, at a potential where PGM anodes still struggle to initiate the reaction (they promote fast HER, this negative current overwhelming any anodic BOR contribution in this potential region). Besides high Ni surface area and metallic surface state, an efficient DBFC anode must have sufficiently large and open pores to ensure efficient mass-transport of reactants and products and optimize the residence time³⁹. We build on recent publication of Braesch *et al.*⁴⁰ to clean NFT from Ni oxides by acid etching (AE) and then modify its surface by Ni electrodeposition (ED). Finally, a unit $\text{BH}_4^-/\text{H}_2\text{O}_2$ DBFC is assembled using these components, whose performance surpass all previous art, reaching record-high open-circuit voltage (2 V) and peak power density (446 $\text{mW}\cdot\text{cm}^{-2}$) for a 5 cm^2 cell.

Experimental

The detailed methods for preparing the Ni-based anode and the AEI can be found in Ref.⁴⁰ and Refs.^{19,27}, respectively.

¹ The value calculated taking into account the unavoidable junction potential between the acidic anode and alkaline cathode compartments.⁵⁸

Nickel-Felt characterization. The support used for the Ni_{ED}/eNFT anodes is a commercial NFT from Sorapec® composed of randomly-dispersed polycrystalline Ni wires (20 μm thick) forming a 500 μm-thick felt. The X-Ray Energy-Dispersive Spectra (XEDS) (EDAX® OCTANE ELITE 25) of the initial NFT and X-Ray Diffraction (XRD) diagrams (Bruker® D8 ADVANCE Diffractometer) of the NFT can be found in electronic supporting information (Figure SI 1 and Figure SI 2, respectively). The felt was imaged by SEM (Zeiss® Gemini SEM-500 operating at 15 or 3 kV) in both Secondary Electron (SE) and Back-Scattered Electron (BSE) mode at each step of the elaboration procedure of the SEBS/Ni_{ED}/eNFT electrodes.

Half-cell measurements. All the electrochemical characterisations were performed in a homemade gas-tight three-electrode glass-cell using either a Biologic VMP-2 or a Gamry REF 600 potentiostat. A 1 M NaOH solution prepared from NaOH crystals (99.999% purity, Merck Suprapur®) dissolved in ultra-pure water (18.2 MΩ, < 3 ppb total organic carbon, MilliQ-gradient + Elix, Millipore®) was used as supporting electrolyte and contained in a PTFE beaker inserted in the glass-cell to avoid contamination of the solution by silicates or other impurities⁴¹. A homemade Reversible Hydrogen Electrode (RHE) freshly-prepared prior each measurement was used as reference electrode and a Pt mesh as the counter-electrode. For the comparative tests (Figure 2) the working electrode was a Glassy Carbon (GC) electrode tip connected to a Rotating Disk Electrode (RDE) (Origatrod®, Orignalys). The commercial carbon-supported nanoparticles (NPs/C, Premetek®) catalysts were all dispersed in isopropanol, water and Nafion to form an ink. A drop of this ink was then deposited on the GC surface to form a thin layer of catalyst with a loading of 40 wt.%. All samples were conditioned in supporting electrolyte by 10 cycles at 100 mV.s⁻¹ followed by 3 cycles in the same potential range at 20 mV.s⁻¹ in order to remove possible impurities. The potential range of the conditioning step did depend on the catalysts: -0.2; 0.4 V vs RHE for Ni-based samples and -0.2; 1.3 V vs RHE for PGM samples. To test the BOR activity of each catalyst, 50 mM of NaBH₄ (98+% Merck®) was added to the 1 M NaOH solution. The solutions were purged by either Ar (99.999% purity) or N₂ (99.999% purity) and CVs were performed in the low potential range (-0.2 → 0.3 V vs RHE) at 20 mV.s⁻¹ at room temperature (*T* = 20°C) and a rotation rate of the RDE of 1600 rpm.

The NFT electrodes were characterized in their initial state and after 90 s of AE without agitation in a mixture of strong acid: 50% of CH₃COOH (glacial, Carl Roth®), 30% HNO₃ (>65%, Carl Roth®), 10% H₂SO₄ (96%, Carl Roth®), 10% H₃PO₄ (>85%, Sigma Aldrich®). This solution was found efficient to remove the top layer of Nickel foams by Grdeń *et al.*^{42,43}.

Ni NPs ED was performed in a separate electrochemical cell of the same design, where a solution of 0.01 M (for electrodeposition on the 0.196 cm_{geo}² RDE electrodes) or 0.1 M (for 5 cm_{geo}² DBFC anodes) NiSO₄ • 6 H₂O (99.97%, Alfa Aesar) + 0.1 M (NH₄)₂SO₄ (99+%, Alfa Aesar) was used as the electrodeposition bath. The ED procedure is described in details in Refs^{29,40}.

Preparation of the SEBS55 polymer and deposition on Ni-based anodes. The preparation of the SEBS55 polymer has been reported in Refs^{19,27}. The solution of chloromethylated SEBS55 (55:45 molar ratio of styrene to rubber) in chlorobenzene was used to coat the Ni_{ED}/eNFT anodes by two methods. The first one is directly adapted from the coating technique used by Wang *et al.*²⁷ and consists of spraying the SEBS solution directly onto the previously-prepared Ni_{ED}/eNFT electrode using an air brush (Badger model 150) fed by nitrogen (N₂, 99.999% purity). The sample is placed on a heating plate (70°C) to evaporate remaining water present in the thickness of the felt and also to evaporate the chlorobenzene, producing a layer of SEBS-55 on the Ni_{ED} NPs. Once the polymer sprayed on the surface, the sample was immersed in a solution of 1-methyl-2-pyrrolidinone (NMP) (20 mL) and TMA (31–35 wt% in ethanol) (5 mL) at 50°C for 24 hours to functionalize it and yield the AEI (SEBS55-TMA). The second method consists of immersing the prepared Ni_{ED}/eNFT electrode in the solution of chloromethylated SEBS55 + chlorobenzene for 10 min. The chlorobenzene has to be removed from the pores prior to the functionalization step in NMP + TMA. To that goal, a drying step of 1 h in a vacuum oven at 60°C has been added after the immersion. The vacuum is mandatory in order to avoid heating the metallic Ni electrode in presence of O₂ and therefore to avoid its irreversible oxidation. Once the sample is dry, the same functionalization step described previously is performed. Prior to the installation of the anode in the cell, it is cleaned with deionized water and then immersed in 1 M KOH for 1 h at room temperature to replace the Cl⁻ moieties by OH⁻.

DBFC (BH₄/H₂O₂) tests. The DBFC measurements were performed at 70°C in a corrosion-resistant cell (Fuel Cell Technologies, Inc.) composed of squared 5 cm² electrodes (2.24 x 2.24 cm) with interdigitated canals. The optimum temperature of *T* = 70°C was chosen as it resulted in the best balance between DBFC performance and minimization of unwanted side reactions (optimization data presented in Figure SI 3). The anodes used were the Ni_{ED}/eNFT+AEI samples described above and the cathode was made of a carbon-supported Pt catalyst (46 wt% Pt/C from Tanaka K. K.) sprayed on porous carbon paper (GDL 24AA diffusion media from Ion Power) resulting in a catalyst loading of 1 mg.cm⁻². A commercial Nafion-117 (175 μm thick) membrane was used to separate the two electrodes and ensure H⁺ conduction. The anolyte was made of 3 M KOH + 1.5 M NaBH₄ and the catholyte of 15 wt% H₂O₂ in 1.5 M H₂SO₄ and both were flowed through the cell using peristaltic pumps with a flow rate of 5 mL.min⁻¹. The flowrate has also been previously optimized⁴⁴ The measurements were performed using a Solartron® potentiostat with a 4 A limitation. 0.1 V decreasing steps were applied and maintained for 2 min from the OCV value to 0.05 V or until the current limitation was reached. In the initial tests, a 200 μm-thick seal was used at the anode, therefore compressing it by 150% and non-negligibly limiting mass-transport in the electrode. Further tests were performed with a 400 μm-thick seal compressing the anode by 25% and allowing a much better transport of the electrolytes in the pores.

Results and discussion

Preparation procedure of enhanced Ni-felts (NFT). The NFT was chosen as the electrode support in order to (i) avoid the use of carbon, the latter leading to durability issues when used in alkaline medium^{45–47}, (ii) increase the overall electronic conductivity of the electrode, but most importantly (iii) provide a better fuel management thanks to its high porosity, one of the key factors for a high-performance DBFC anode³⁹. The NFT in its pristine state is ill-suited for a DBFC anode. The elaboration procedure to obtain a high-performance anode is detailed in Ref.⁴⁰ and Figure 1 summarizes the state of the NFT after each of the electrode elaboration step. The cyclic voltammogram (CV, Figure 1.A) shows the electrochemical signature of the electrode in supporting electrolyte. Cyclic voltammetry is a facile *in situ* tool, which allows not only to probe the state of the Ni surface (metallic versus oxide-covered), but also to quantify the amount of **metallic sites** available on the surface, and to determine the available Electrochemical Surface Area (ECSA) of metallic Ni.² This is conveniently done by integrating the CV peak observed around 0.3 V vs RHE and corresponding to the transition between Ni and surface α -Ni(OH)₂.^{29,40,48} For a pristine NFT, no peak is observed at 0.3 V, a sign of strongly-oxidized surface (either resulting from the NFT manufacturing or ambient storage). This translates into poor BOR activity (Figure 1.B) as explained in Ref.²⁹ AE of the NFT in a mixture of strong acids (described by Grdeń *et al.*^{42,43}) aimed to remove the oxidized layers and efficiently reveals the underneath metallic sites: SEM images of the etched-NFT (eNFT)

show a rougher surface, demonstrating that nickel oxides were (at least partially) removed/dissolved. The CV of Figure 1.A reveals an increased double layer capacitance and the emergence of a peak at 0.3 V vs RHE, which confirms the presence of metallic nickel sites on the surface; as a result, the BOR activity increases (Figure 1.B). This BOR activity is however still not sufficiently high for the DBFC, because the amount of active sites is limited by the surface of the NFT. Further increasing the NFT roughness by AE would lead to excessive nickel fibre thinning, degradation of the felt mechanical strength, and failure of the anode material's integrity. To substantially increase the number of active sites, the best option is to perform an ED of Ni NPs. The procedure was developed by some of us^{29,36,49} and adapted to the eNFT (Ni_{ED}/eNFT). The SEM images of Figure 1 present the resulting surface, where Ni-agglomerates can now be observed. Ni-electrodeposition on the NFT results in 8.5-fold increase of the number of metallic surface sites (ECSA of 1942 cm² after the Ni_{ED} against 227 cm² before the ED), which translates in very fast BOR kinetics and low onset-potential (-220 mV vs RHE). The amount of electrodeposited Ni cannot be calculated from the deposition charge, because of the H₂ formation (through HER) occurring simultaneously to the Ni²⁺ reduction at the deposition potential. Whereas the nickel-loading of the Ni_{ED}/C could be measured using ICP-MS analyses²⁹, this method cannot be applied to the Ni_{ED}/eNFT samples (because of the NFT). However, using the ECSA values, the loading of the 1942 cm² Ni_{ED}/eNFT electrode was estimated as 1.2 mg_{Ni,ED}·cm⁻²

² Note that the information provided by CV regarding the surface state of Ni and the number of metallic Ni sites is much more precise than that offered by *ex situ* X-ray photoelectron spectroscopy.

ARTICLE

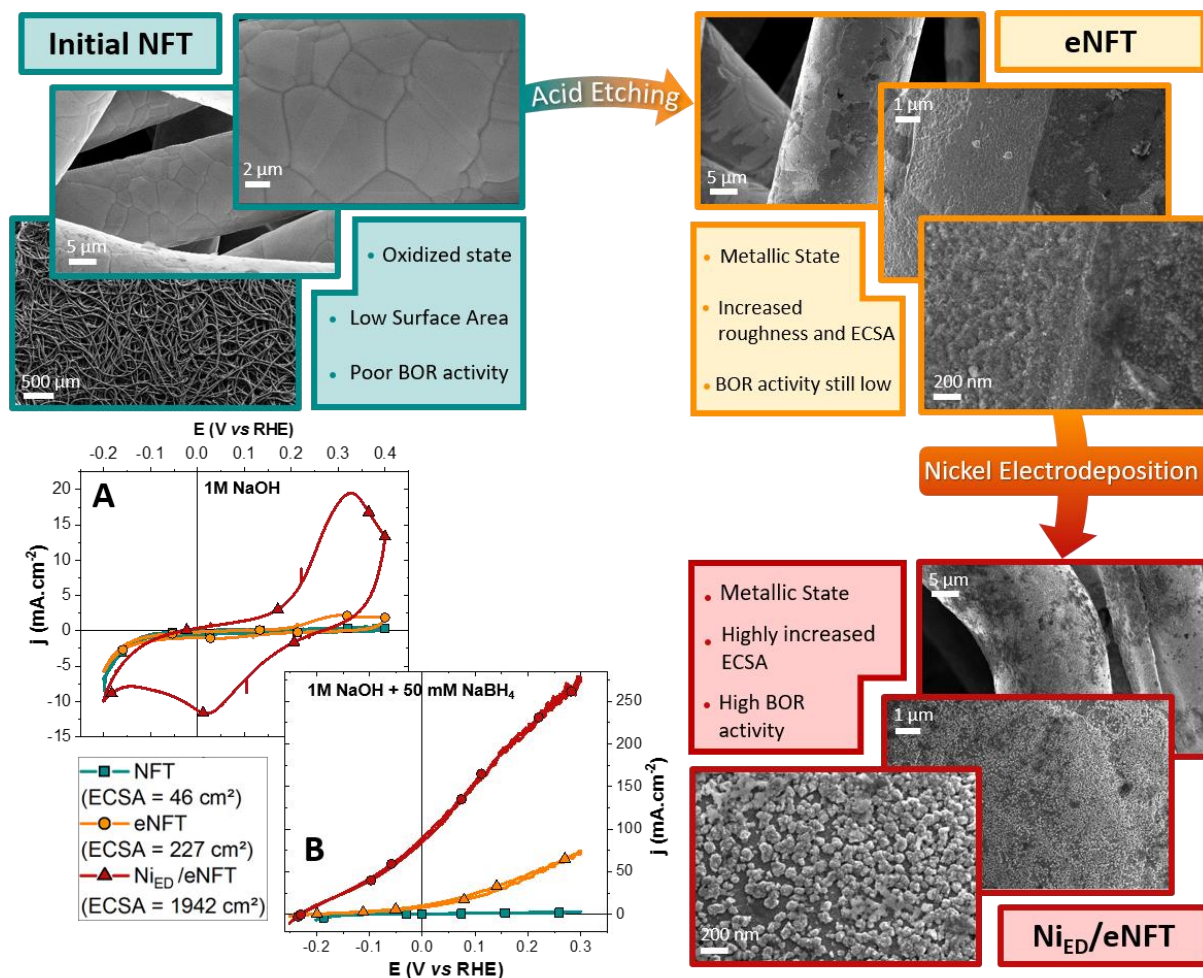


Figure 1. Evolution of the morphology, electrochemical surface area (ECSA), and BOR activity following consecutive steps of the electrode elaboration process. The oxidation state and the amount of active sites is tuned through a two-steps process: (i) an acid etching of the initial NFT to reveal metallic sites and increase the roughness (ii) and an electrodeposition of Ni NPs to highly increase the number of active sites and the BOR activity, as demonstrated by voltamograms both in (A) supporting electrolyte (1 M NaOH) and in (B) BOR conditions (1 M NaOH + 50 mM NaBH₄). CV conditions: Ar-saturated solutions, $T = 20^{\circ}\text{C}$, $v_s = 20 \text{ mV}\cdot\text{s}^{-1}$, $\omega = 1600 \text{ rpm}$.

Comparison of Ni_{ED}/eNFT anodes with state-of-the-art BOR catalysts. In order to benchmark the outstanding BOR activity of the so-obtained Ni_{ED}/eNFT anodes, they were tested in a half-cell configuration in both potentiodynamic and potentiostatic conditions and compared to other Ni-based catalysts: Ni_{ED}/C from Ref.²⁹ and Ni/C NPs (provided by Prof. Deckel's group⁵⁰ and obtained through wet chemical synthesis followed by relevant heat-treatments to first reduce Ni²⁺ and then passivate the ensuing Ni nanoparticles); PGM catalysts (commercial Pt/C, Pd/C) and Au/C NPs, the most commonly-used electrocatalysts for the BOR, were also tested for comparison. The potentiodynamic measurement (Figure

2.A) highlights the low onset potential of Ni electrodeposited either on carbon or Ni felt, while representative potentiostatic measurements (Figure 2.B) demonstrate the stability of the current at a given potential. Pt is still the most used BOR catalyst, owing to the high current densities obtained at its surface, albeit at potential values above 0 V vs RHE. However, this current (at least partly) comes from the indirect oxidation of the H_{ad} species formed on the Pt surface during the dissociative adsorption of BH₄⁻⁵¹⁻⁵³. In addition, the high activity of Pt towards hydrogen electrode reactions drags the mixed potential of a NaBH₄-containing electrolyte towards the equilibrium hydrogen electrode potential (0 V vs. RHE), thus

preventing the BOR onset potential to approach the thermodynamic value (the BOR onset on Pt is -50 mV vs RHE in 50 mM NaBH₄, Figure 2.A). On the contrary, because of the poor HER activity of metallic Ni, the Ni_{ED}/C catalyst shows a significantly-lower onset potential (-250 mV vs RHE in 50 mM NaBH₄, Figure 2.A) and fast BOR kinetics, making of metallic-Ni the best BOR catalyst in the low potential region (the most practically-relevant region for a DBFC anode). While the 200 mV OCV improvement has been reported in Refs.^{29,40}, the limiting current on the Ni_{ED}/C electrode was inferior to that of Pt/C, resulting in an overall 4 electrons generated per BH₄⁻ species. The Ni_{ED}/eNFT electrode presents the same BOR activity at low potentials, owing to its metallic surface-state, but mass-transfer limitation (evident with Ni_{ED}/C) is now less pronounced and the current density competes with Pt/C until higher potential values. This shows that using a very open 3D NFT structure as the NPs support, enables better mass-transfer and management of intermediate species⁴⁰. The Ni/C catalyst prepared by a *conventional* chemical synthesis (involving heat-treatments during the reduction step), followed by surface passivation of the Ni NPs⁵⁰ shows higher onset potential, but most importantly much slower reaction kinetics. Indeed, the mandatory passivation step of the preparation procedure (otherwise the material is pyrophoric) and (inevitable) storage/transport under air

(which can be avoided with the electrodeposition procedure), lead to highly-oxidized Ni NPs. This surface oxidation is hardly reversible: even after conditioning in supporting electrolyte and attempts to reduce the surface in strongly-reducing BH₄⁻ conditions (or at low electrode potentials), the samples cannot be activated. Both Pd/C and Au/C show really poor performance towards the BOR in the low potential range. Potentiostatic measurements shown in Figure 2B are more relevant to the DBFC operation conditions. While the Pt/C electrode slightly outperforms Ni electrodes in terms of the initial current density at potential equal to or higher than 0.2 V vs RHE, a significant current drop is observed (more than 90% in 1 hour) when the potential is maintained at 0.2 V vs RHE (Figure 2.B). This effect, exacerbated at high NaBH₄ concentration²⁹, is explained by the self-poisoning of the electrode by the BOR intermediate species^{54,55}, which progressively block its active sites. Such poisoning is not observed on metallic Ni surfaces or at least to a much lesser extent, due to a weaker BH₄⁻ adsorption corroborated by DFT calculations²⁹, suggesting that the BOR proceeds *via* a different reaction pathway generating less poisoning species. Thus, metallic Ni-based electrodes are more stable towards the BOR, a clear advantage for DBFC applications.

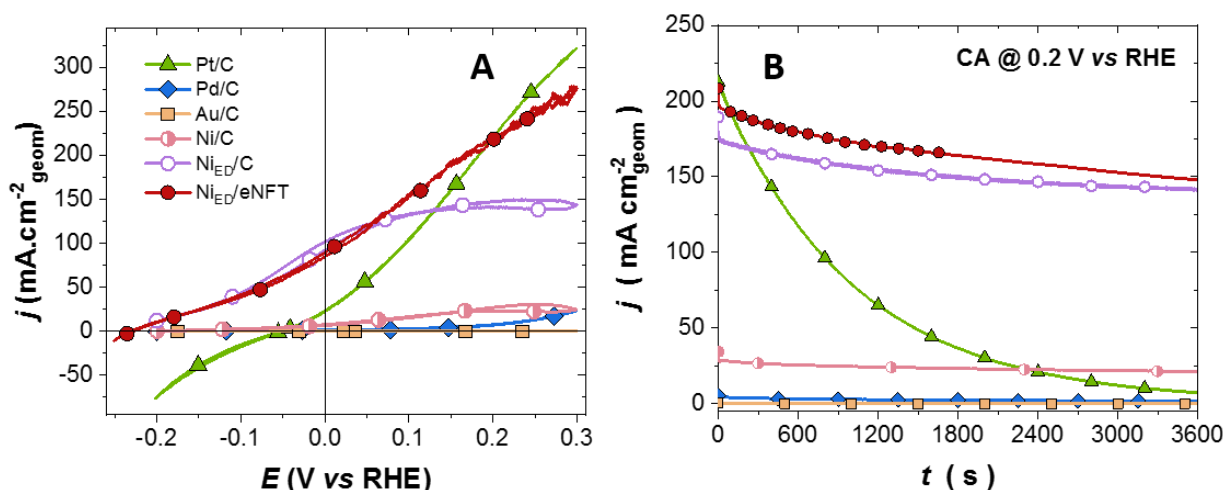


Figure 2. Comparison of the most commonly used catalysts for the BOR and the Ni_{ED}-based electrodes in 1 M NaOH + 50 mM NaBH₄ (Ar-saturated solution, $T = 20^\circ\text{C}$, $\omega = 1600$ rpm) in: (A) potentiodynamic conditions ($v_s = 20$ mV.s⁻¹) showing the lower onset potential on Ni_{ED}-based catalysts compared to PGMs and (B) potentiostatic conditions ($E = 0.2$ V vs RHE) showing the better stability on Ni_{ED}-based catalysts. The metal loading for all electrodes is $40 \mu\text{g.cm}^{-2}$.

Deposition of an anion exchange ionomer (AEI) on Ni_{ED}/eNFT anodes. Deposition of the AEI layer on the DBFC anode is an essential step in the elaboration of a PMBI,²⁷ the latter ensuring efficient separation of the alkaline anolyte and acidic catholyte. Considering the influence of the state of the Ni surface on its BOR activity, the challenge was to develop a deposition procedure ensuring uniform coating, while maintaining the reduced (metallic) state of the Ni_{ED}/eNFT anode. Several deposition procedures have been evaluated and compared. The spraying method (in what follows

labelled with S) was adapted from Wang et al²⁷, where it was applied to a Pd/C DBFC anode. After the ED of Ni NPs, the sample was dried using absorbent paper and then placed on a heating plate (70°C) and the SEBS55 polymer (see Refs. ^{19,27}) was sprayed directly on it, water being still present in the pores, and chlorobenzene solvent evaporated. After the coating, the SEBS55 was functionalized in NMP + TMA, yielding the AEI. The SEM images are presented on Figure 3 (red frame) together with the current-voltage characteristics and the power density. The electrodes were tested in DBFC conditions using a commercial Nafion-117[®] membrane and a Pt/C (1 mg.cm^{-2}) cathode for H₂O₂ reduction.

ARTICLE

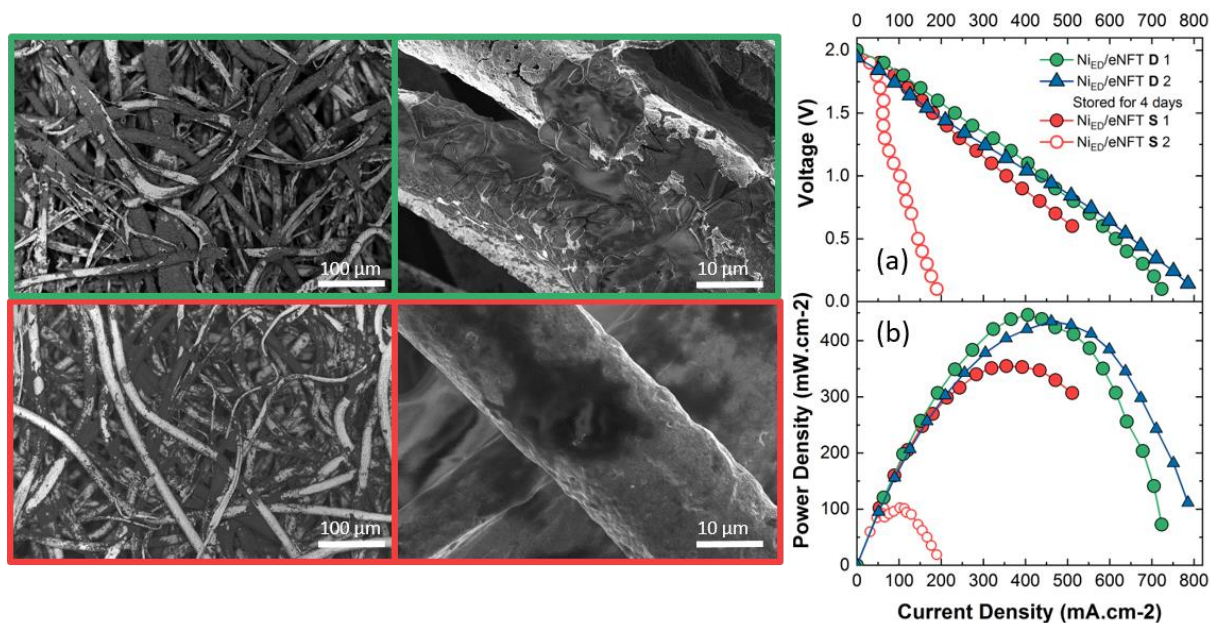


Figure 3. SEM images of the SEBS/Ni_{ED}/eNFT electrodes prepared via either dipping (D) of the anode in SEBS-55 solution (green borders) or spraying (S) of the ionomer solution onto the electrode (red borders) at different magnification (x 200 and x 5k). Corresponding polarization (a) and power density (b) curves in DBFC conditions of the two preparation methods ($T = 70^{\circ}\text{C}$, anolyte: 3 M KOH + 1.5 M NaBH₄, catholyte: 1.5 M H₂SO₄ + 15 wt.% H₂O₂, flow rate: 0.4 mL·min⁻¹·cm⁻²). The SEM images were acquired after DBFC measurements in which the anode was pressed against the membrane. The AEI layer directly in contact with it was therefore essentially removed from the anode when it was separated from the membrane. This explains why most of the outer nickel wires appears without the AEI layer, but the ionomer was most probably present before and during the DBFC tests.

The Ni_{ED}/eNFT-S 1 anode reached an impressive OCV of 2.0 V (red curve in Figure 3), where only 1.8 V was reached in the same conditions using Pd/C anodes²⁷. This corresponds to the 200 mV improvement measured on metallic Ni surfaces compared to PGM catalysts during the half cell tests. Reaching this improvement firstly confirms the effectiveness of the PMBI to maintain the important pH gradient between the anode and the cathode (the slope of the polarisation plot is parallel to the one with Pd/C from,²⁷ where the film integrity was confirmed). Secondly, it means that the anode is indeed capable to oxidize the BH₄⁻ at very low potential (lower than what Pd can do), hence that Ni is in its mostly-reduced state. The peak power density for the Ni_{ED}/eNFT-S 1 sample was achieved at 1.0 V and reached 355 mW cm⁻². One must remember that spraying was performed in air at $T = 70^{\circ}\text{C}$, conditions where the surface of Ni nanoparticles might be partly-oxidized, so this performance is already outstanding. A second electrode was prepared in the exact similar conditions (Ni_{ED}/eNFT-S 2) and the same OCV was reached, meaning that the state of surface of the anode is still metallic, in majority. However, this second test showed a disastrous peak power density ($P_{\text{max}} = 102 \text{ mW}\cdot\text{cm}^{-2}$ at 1.0 V). This is attributed to a non-reproducibility in the spraying deposition method: (i) it is almost

impossible to assert that the sprayed AEI layer fully penetrates the whole thickness of the Ni_{ED}/eNFT, leaving uncoated Ni fibres for which the PMBI is not well-established and the Ni-metal state of surface might be locally-lost, while (ii) in some cases, fibres might be surrounded by thick pockets of AEI, thereby preventing mass-transfer of reactant to the Ni catalytic sites, and inhibiting the necessary release of hydrogen bubbles formed in the bulk of the porous electrode. In order to solve this issue, another method, namely dipping (in what follows labelled as D) was evaluated. To this end, the Ni_{ED}/eNFT was simply dipped (at room temperature) in the solution of SEBS-55 in chlorobenzene after removing any excess of water (by gentle pressing of the electrode on an absorbent paper) to allow solvent penetration in the Ni_{ED}/eNFT pores. Then, the AEI layer was dried for 1 h in a vacuum oven at $T = 60^{\circ}\text{C}$, vacuum (absence of O₂) preventing irreversible oxidation of the Ni_{ED}/eNFT. This strategy enables more homogeneous coating of the AEI in the whole Ni_{ED}/eNFT structure (which prevents the biases noted for the dipping method, above) while preserving the metallic state of the electrode as confirmed by the high OCV value. As such, the dipping procedure resulted in reproducible anodes, leading to OCV values of 2.0 V and a yet higher peak power density of ca. 450 mW cm⁻². This confirms the

importance of the AEI deposition procedure for the overall performance and suggests that the targeted metallic surface state of the Ni_{ED}/eNFT-D 1 electrode was indeed achieved. This method resulted in a more reproducible ionomer deposition as attested by the comparable performance obtained with both electrodes prepared this way (Figure 3), although the coating was not strictly homogenous on the entire surface. Moreover, this second electrode (Ni_{ED}/eNFT-D 2) was stored in water for four days prior to the DBFC

test. While exhibiting somewhat lower OCV (1.94 V, likely due to formation of some surface oxides on the Ni surface during the electrode storage), the latter shows comparable overall performance (blue curve), thus confirming that the developed approach is fully-compatible with practical applications, where exposure to air may be inevitable (a result of utmost importance). Previous publications^{27,56} demonstrated stability of PMBI under similar operating conditions.

Table 1. Comparison of recent DBFC performance data. “na” stand for non-available information.

Ref	Anode (loading, mg.cm ⁻²)	Cathode (loading, mg.cm ⁻²)	Separator (thickness, μm)	Oxidant	T (°C)	P _{max} (mW.cm ⁻²)	OCV (V)
39	Pt/C(0.5)	Pt/C (2)	Nafion 212 (50)	O ₂	60	420	0.94
31	NiB/C (70)	LaNi _{0.9} Ru _{0.1} O ₃ /C (7.5)	PEM (na)	O ₂	25	180	1.09
57	Pd/C (0.3)	Pt/C (0.3)	Nafion 117 (183)	H ₂ O ₂	25	211	1.72
57	Pt/C (0.3)	Pt/C (0.3)	Nafion 117 (183)	H ₂ O ₂	25	275	1.67
29	Ni _{ED} /C (0.6)	Pt/C (2)	Nafion 212 (50)	O ₂	60	108	1.21
40	Pt/C (0.16)	Pt/C (2)	Nafion 212 (50)	O ₂	60	194	1.01
40	Ni _{ED} /eNFT (1.2)	Pt/C (2)	Nafion 212 (50)	O ₂	60	180	1.24
27	Pd/C(1)+Ni	Pt/C (1)	Bipolar Interface (175)	H ₂ O ₂	70	300	1.80
This work	Ni _{ED} /eNFT-D (0.7)	Pt/C (1)	Bipolar Interface (175)	H ₂ O ₂	70	446	2.0

Benchmarking the DBFC performance. The OCV (2.0 V) and peak power density (446 mW.cm⁻²) reached with the Ni_{ED}/eNFT-D anodes confirm the advantageous combination of the PMBI, the high-surface area 3D-open structure metallic Ni catalyst and the optimized AEI deposition procedure: this impressive result largely surpasses that of a PGM-based cell (with the same geometry and operating conditions), as displayed on Figure 4. Additional comparative values of peak power density and OCV with recently-published studies are listed in Table 1, corroborating the unprecedented performance of BH₄⁻/H₂O₂ DBFC achieved in this work using non-PGM anode catalysts. The improvement of 200 mV on the OCV by using Ni electrodes (in their metallic state of surface) over Pt or Pd is clearly observed with either O₂ or H₂O₂ oxidant. Ni-based anodes perform better at high cell voltage in both conditions, and are tied (within the error bar) with Pt anodes combined with a CEM and O₂ at the cathode. In addition, the power density drops more abruptly at high current density with Pt/C than with Ni_{ED}/eNFT, which can be associated with more efficient mass-transfer in the open porosity 3D-structured NFT support than in “compact” carbon black-based active layers. Regarding the PMBI + H₂O₂ results, polarization curves for Ni_{ED}/eNFT-D and Pd/C are rather parallel, signing the overall better catalytic performance of Ni_{ED}/eNFT versus Pd/C (all other limitations, e.g. related to Ohmic drop and mass-transfer, being identical). The slope of the polarization curves for the PMBI cells is however steeper in these conditions. This is explained by the use of a significantly thicker (175 μm) Nafion-117 membrane than the one used during the O₂ tests (Nafion-212, 50 μm). While using thinner CEM would lower the cell resistance and therefore improve its performance, it could

lead to larger risks of membrane perforation and of mixing of the strongly-reducing alkaline anolyte with a strongly-oxidizing acidic catholyte, adversely-affecting the durability of the cell.

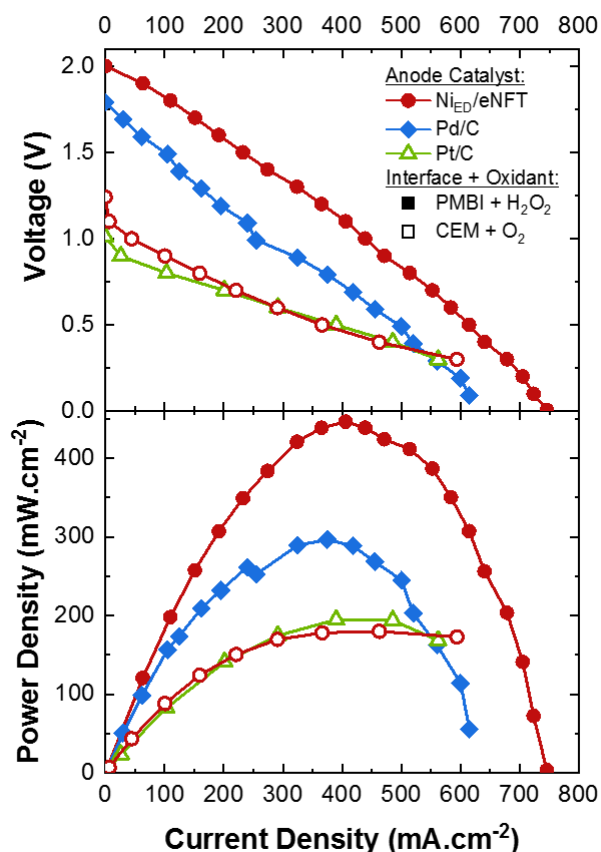


Figure 4. DBFC performance of $\text{Ni}_{\text{ED}}/\text{eNFT}$ anodes used in two different configurations: PMBI separator + H_2O_2 oxidant at $T = 70^\circ\text{C}$ compared to Pd anode (full symbols), CEM and O_2 oxidant at $T = 60^\circ\text{C}$ compared to Pt anode (hollow symbols) Commercial Pt/C electrodes ($1 \text{ mg}\cdot\text{cm}^{-2}$) are used at the cathodes in all configurations. Pd/C data was reproduced from Ref.²⁷ with permission from Nature-Springer and CEM+ O_2 data was reproduced from Ref.⁴⁰ with the permission from Wiley.

Conclusion

In this study, we take advantage of the use of electrodeposited metallic nickel as an effective and cheap catalyst to increase the BOR activity at high cell voltage, an open 3D stand-alone electrode structure brought by a Ni felt to favour mass-transfer of reactants/products, and of a pH-gradient-enabled microscale bipolar interface (PMBI) to efficiently separate the anolyte and catholyte compartments of a $\text{BH}_4^-/\text{H}_2\text{O}_2$ fed DBFC. This unique combination enables to reach unprecedented performance: OCV (2.0 V) and peak power density ($446 \text{ mW}\cdot\text{cm}^{-2}$) for a $\text{BH}_4^-/\text{H}_2\text{O}_2$ fed DBFC. The use of the anion-exchange ionomer at the anode deposited in a tailored procedure proved to be effective to protect the metallic $\text{Ni}_{\text{ED}}/\text{eNFT}$ anode towards extensive and irreversible oxidation, while the $\text{Ni}_{\text{ED}}/\text{eNFT}$ anode structure/composition maintained its promises in practical $\text{BH}_4^-/\text{H}_2\text{O}_2$ fed DBFC compared to model 3-electrode cell

measurements. This work opens the way to high-performance non-PGM based $\text{BH}_4^-/\text{H}_2\text{O}_2$ fed DBFC, for portable applications.

Data availability.

The data that support the plots within this paper and other findings of this study are available from the corresponding authors upon reasonable request.

Acknowledgements

This work has been performed in the frame of the MobiDiC project, funded by the French National Research Agency (ANR, grant # ANR-16-CE05-0009-01). The authors express their gratitude to R. Martin, T. Encinas, for their support in SEM, EDS, XRD characterization and to Prof. Deckel's group for providing Ni/C catalysts.

A.O. acknowledges the financial support from the RSF project No. 18-73-00143, funded by the Russian Science Foundation.

Z.W., S.S. and V.R. would like to acknowledge with gratitude the Office of Naval Research (ONR grant number N00014-16-1-2833) for funding their portion of this work. V.R. acknowledges with gratitude generous support from the Roma B. and Raymond H. Wittcoff Distinguished University Professorship.

MC and GB thank Elena Davydova and Dario R. Dekel (Technion, Haifa, Israel) for having gently provided the Ni/C catalyst used as benchmark in Fig. 2.

Author contributions

GB and MC had the original idea of the study and planned the experiments; ES, AB and VR also contributed to the experiments' planning. GB made most of the experiments, data analysis (with MC) and drafted the first version of the paper. ZW and SS contributed to the DBFC ($\text{BH}_4^-/\text{H}_2\text{O}_2$) tests. AO contributed to the preparation of the Ni_{ED} samples. All authors contributed to the manuscript revision. MC and GB prepared the final version of the article.

Conflicts of interest

The authors have no conflicts of interest to declare.

References

1. Li, Z. P., Liu, B. H., Arai, K., Asaba, K. & Suda, S. Evaluation of alkaline borohydride solutions as the fuel for fuel cell. *J.*

- Power Sources* **126**, 28–33 (2004).
2. Park, K. T., Jung, U. H., Jeong, S. U. & Kim, S. H. Influence of anode diffusion layer properties on performance of direct borohydride fuel cell. *J. Power Sources* **162**, 192–197 (2006).
 3. Miley, G. H. *et al.* Direct NaBH₄/H₂O₂ fuel cells. *J. Power Sources* **165**, 509–516 (2007).
 4. Demirci, U. B. Direct liquid-feed fuel cells: Thermodynamic and environmental concerns. *J. Power Sources* **169**, 239–246 (2007).
 5. Molina Concha, B. & Chatenet, M. Direct oxidation of sodium borohydride on Pt, Ag and alloyed Pt-Ag electrodes in basic media. Part II. Carbon-supported nanoparticles. *Electrochim. Acta* **54**, 6130–6139 (2009).
 6. Urian, R. C. Air Independent Fuel Cells Utilizing Borohydride and Hydrogen Peroxide. *Mater. Res. Soc. Symp. Proc. Vol. 1213*, (2010).
 7. Liu, B. H. & Li, Z. P. Current status and progress of direct borohydride fuel cell technology development. *J. Power Sources* **187**, 291–297 (2009).
 8. Ma, J., Choudhury, N. A. & Sahai, Y. A comprehensive review of direct borohydride fuel cells. *Renewable and Sustainable Energy Reviews* **14**, 183–199 (2010).
 9. Choudhury, N. A., Raman, R. K., Sampath, S. & Shukla, A. K. An alkaline direct borohydride fuel cell with hydrogen peroxide as oxidant. *J. Power Sources* **143**, 1–8 (2005).
 10. Cao, D., Gao, Y., Wang, G., Miao, R. & Liu, Y. A direct NaBH₄-H₂O₂ fuel cell using Ni foam supported Au nanoparticles as electrodes. *Int. J. Hydrogen Energy* **35**, 807–813 (2010).
 11. Haijun, W., Cheng, W., Zhixiang, L. & Zongqiang, M. Influence of operation conditions on direct NaBH₄/H₂O₂ fuel cell performance. *Int. J. Hydrogen Energy* **35**, 2648–2651 (2010).
 12. Oh, T. H. Design specifications of direct borohydride–hydrogen peroxide fuel cell system for space missions. *Aerosp. Sci. Technol.* **58**, 511–517 (2016).
 13. Andrieux, J. *et al.* Spontaneous hydrolysis of sodium borohydride in harsh conditions. *Int. J. Hydrogen Energy* **36**, 224–233 (2011).
 14. Demirci, U. B. *et al.* Sodium Borohydride Hydrolysis as Hydrogen Generator: Issues, State of the Art and Applicability Upstream from a Fuel Cell. *Fuel Cells* **10**, 335–350 (2010).
 15. Yamada, K. *et al.* Investigation of PEM type direct hydrazine fuel cell. *J. Power Sources* **115**, 236–242 (2003).
 16. Duteanu, N., Vlachogiannopoulos, G., Shivhare, M. R., Yu, E. H. & Scott, K. A parametric study of a platinum ruthenium anode in a direct borohydride fuel cell. *J. Appl. Electrochem.* **37**, 1085–1091 (2007).
 17. Coowar, F. A., Vitins, G., Mepsted, G. O., Waring, S. C. & Horsfall, J. A. Electrochemical oxidation of borohydride at nano-gold-based electrodes: Application in direct borohydride fuel cells. *J. Power Sources* **175**, 317–324 (2008).
 18. Qu, C., Zhang, H., Zhang, F. & Liu, B. A high-performance anion exchange membrane based on bi-guanidinium bridged polysilsesquioxane for alkaline fuel cell application. *J. Mater. Chem.* **22**, 8203–8207 (2012).
 19. Wang, Z., Parrondo, J. & Ramani, V. Anion Exchange Membranes Based on Polystyrene- Block -Poly(ethylene-ran -butylene)- Block -Polystyrene Triblock Copolymers: Cation Stability and Fuel Cell Performance. *J. Electrochem. Soc.* **164**, F1216–F1225 (2017).
 20. Simons, R. Preparation of a high performance bipolar membrane. *J. Memb. Sci.* **78**, 13–23 (1993).
 21. Bazinet, L., Lamarche, F. & Ippersiel, D. Bipolar-membrane electro dialysis: Applications of electro dialysis in the food industry. *Trends Food Sci. Technol.* **9**, 107–113 (1998).
 22. Xu, T. Development of bipolar membrane-based processes. *Desalination* **140**, 247–258 (2001).
 23. Dai, J. *et al.* A sandwiched bipolar membrane for all vanadium redox flow battery with high coulombic efficiency. *Polymer (Guildf)*. **140**, 233–239 (2018).
 24. de León, C. P. *et al.* A direct borohydride-Acid peroxide fuel cell. *J. Power Sources* **164**, 441–448 (2007).
 25. Reeve, R. W. A Sodium Borohydride-Hydrogen Peroxide Fuel Cell Employing a Bipolar Membrane Electrolyte. *Fuel Cell Semin.* **2011** **42**, 117–129 (2012).
 26. Arges, C. G., Prabhakaran, V., Wang, L. & Ramani, V. Bipolar polymer electrolyte interfaces for hydrogen-oxygen and direct borohydride fuel cells. *Int. J. Hydrogen Energy* **39**, 14312–14321 (2014).
 27. Wang, Z., Parrondo, J., He, C., Sankarasubramanian, S. & Ramani, V. Efficient pH-gradient-enabled microscale bipolar interfaces in direct borohydride fuel cells. *Nat. Energy* **4**, 281–289 (2019).
 28. Vesborg, P. C. K. & Jaramillo, T. F. Addressing the terawatt challenge: Scalability in the supply of chemical elements for renewable energy. *RSC Advances* **2**, 7933–7947 (2012).
 29. Oshchepkov, A. G. *et al.* Nickel Metal Nanoparticles as Anode Electrocatalysts for Highly Efficient Direct Borohydride Fuel Cells. *ACS Catal.* **9**, 8520–8528 (2019).
 30. Ma, X. *et al.* Facile fabrication of gold coated nickel nanoarrays and its excellent catalytic performance towards sodium borohydride electro-oxidation. *Appl. Surf. Sci.* **414**, 353–360 (2017).

31. Li, S., Shu, C., Chen, Y. & Wang, L. A new application of nickel-boron amorphous alloy nanoparticles: anode-catalyzed direct borohydride fuel cell. *Ionics (Kiel)* **24**, 201–209 (2018).
32. Zhang, D. *et al.* Three-dimensional functionalized graphene networks modified Ni foam based gold electrode for sodium borohydride electrooxidation. *Int. J. Hydrogen Energy* **41**, 11593–11598 (2016).
33. Hua Dong *et al.* Electrooxidation mechanisms and discharge characteristics of borohydride on different catalytic metal surfaces. *J. Phys. Chem. B* **109**, 10896–10901 (2005).
34. Geng, X., Zhang, H., Ye, W., Ma, Y. & Zhong, H. Ni-Pt/C as anode electrocatalyst for a direct borohydride fuel cell. *J. Power Sources* **185**, 627–632 (2008).
35. Zhang, D. *et al.* Nickel particles supported on multi-walled carbon nanotubes modified sponge for sodium borohydride electrooxidation. *Electrochem. commun.* **35**, 128–130 (2013).
36. Oshchepkov, A. G. *et al.* Exploring the Influence of the Nickel Oxide Species on the Kinetics of Hydrogen Electrode Reactions in Alkaline Media. *Top. Catal.* **59**, 1319–1331 (2016).
37. Oshchepkov, A. G., Bonnefont, A., Parmon, V. N. & Savinova, E. R. On the effect of temperature and surface oxidation on the kinetics of hydrogen electrode reactions on nickel in alkaline media. *Electrochim. Acta* **269**, 111–118 (2018).
38. Oshchepkov, A. G., Bonnefont, A. & Savinova, E. R. On the Influence of the Extent of Oxidation on the Kinetics of the Hydrogen Electrode Reactions on Polycrystalline Nickel. *Electrocatalysis* **11**, 133–142 (2020).
39. Olu, P. Y., Deschamps, F., Caldarella, G., Chatenet, M. & Job, N. Investigation of platinum and palladium as potential anodic catalysts for direct borohydride and ammonia borane fuel cells. *J. Power Sources* **297**, 492–503 (2015).
40. Braesch, G. *et al.* Nickel 3D Structures Enhanced by Electrodeposition of Nickel Nanoparticles as High Performance Anodes for Direct Borohydride Fuel Cells. *ChemElectroChem* **7**, 1789–1799 (2020).
41. Mayrhofer, K. J. J., Crampton, A. S., Wiberg, G. K. H. & Arenz, M. Analysis of the Impact of Individual Glass Constituents on Electrocatalysis on Pt Electrodes in Alkaline Solution. *J. Electrochem. Soc.* **155**, P78 (2008).
42. Grdeń, M., Alsabet, M. & Jerkiewicz, G. Surface Science and Electrochemical Analysis of Nickel Foams. *ACS Appl. Mater. Interfaces* **4**, 3012–3021 (2012).
43. Grdeń, M. & Jerkiewicz, G. Influence of Surface Treatment on the Kinetics of the Hydrogen Evolution Reaction on Bulk and Porous Nickel Materials. *Electrocatalysis* **10**, 173–183 (2019).
44. Wang, Z., Sankarasubramanian, S. & Ramani, V. Reactant-Transport Engineering Approach to High-Power Direct Borohydride Fuel Cells. *Cell Reports Phys. Sci.* **1**, 100084 (2020).
45. Zadick, A., Dubau, L., Sergent, N., Berthomé, G. & Chatenet, M. Huge Instability of Pt/C Catalysts in Alkaline Medium. *ACS Catal.* **5**, 4819–4824 (2015).
46. Lafforgue, C., Zadick, A., Dubau, L., Maillard, F. & Chatenet, M. Selected Review of the Degradation of Pt and Pd-based Carbon-supported Electrocatalysts for Alkaline Fuel Cells: Towards Mechanisms of Degradation. *Fuel Cells* **18**, 229–238 (2018).
47. Lafforgue, C., Chatenet, M., Dubau, L. & Dekel, D. R. Accelerated Stress Test of Pt/C Nanoparticles in an Interface with an Anion-Exchange Membrane - An Identical-Location Transmission Electron Microscopy Study. *ACS Catal.* **8**, (2018).
48. Machado, S. A. S. & Avaca, L. A. The hydrogen evolution reaction on nickel surfaces stabilized by H-absorption. *Electrochim. Acta* **39**, 1385–1391 (1994).
49. Oshchepkov, A. G. *et al.* On the effect of Cu on the activity of carbon supported Ni nanoparticles for hydrogen electrode reactions in alkaline medium. *Top. Catal.* **58**, 1181–1192 (2015).
50. Davydova, E. S., Speck, F. D., Paul, M. T. Y., Dekel, D. R. & Cherevko, S. Stability Limits of Ni-Based Hydrogen Oxidation Electrocatalysts for Anion Exchange Membrane Fuel Cells. *ACS Catal.* **9**, 6837–6845 (2019).
51. Rostamikia, G. & Janik, M. J. Direct borohydride oxidation: mechanism determination and design of alloy catalysts guided by density functional theory. *Energy Environ. Sci.* **3**, 1262 (2010).
52. Rostamikia, G. & Janik, M. J. First principles mechanistic study of borohydride oxidation over the Pt(1 1 1) surface. *Electrochim. Acta* **55**, 1175–1183 (2010).
53. Olu, P.-Y. *et al.* Influence of the concentration of borohydride towards hydrogen production and escape for borohydride oxidation reaction on Pt and Au electrodes – experimental and modelling insights. *J. Power Sources* **375**, 300–309 (2018).
54. Finkelstein, D. A. *et al.* Self-Poisoning during BH 4 – Oxidation at Pt and Au, and in Situ Poison Removal Procedures for BH 4 – Fuel Cells. *J. Phys. Chem. C* **117**, 1571–1581 (2013).
55. Braesch, G., Bonnefont, A., Martin, V., Savinova, E. R. & Chatenet, M. Borohydride oxidation reaction mechanisms and poisoning effects on Au, Pt and Pd bulk electrodes: From model (low) to direct borohydride fuel cell operating (high) concentrations. *Electrochim. Acta* **273**, 483–494 (2018).

ARTICLE

Journal Name

56. Wang, Z. *et al.* Influence of Water Transport across Microscale Bipolar Interfaces on the Performance of Direct Borohydride Fuel Cells. *ACS Appl. Energy Mater.* **3**, 4449–4456 (2020).
57. Hjelm, R. M. E. *et al.* Impact of the Anode Catalyst Layer Design on the Performance of H₂O₂-Direct Borohydride Fuel Cells. *J. Electrochem. Soc.* **166**, F1218–F1228 (2019).
58. Chatenet, M. Tailoring membranes. *Nat. Energy* **4**, 261–262 (2019).